IEEE Access
Multidisciplinary | Rapid Review | Open Access Journal

Received December 3, 2019, accepted January 4, 2020, date of publication January 17, 2020, date of current version February 4, 2020.

Digital Object Identifier 10.1109/ACCESS.2020.2967215

Space-Frequency Index Modulation for Combating ICI in Intelligent Mobility Communications

RUI CAO[1], XIA LEI[1], YUE XIAO[1], (Member, IEEE), YOU LI[1], AND WEI XIANG[2]
[1]National Key Laboratory of Science and Technology on Communications, University of Electronic Science and Technology of China, Chengdu 611731, China
[2]College of Science and Engineering, James Cook University, Cairns, QLD 4878, Australia

Corresponding authors: Xia Lei (leixia@uestc.edu.cn) and Wei Xiang (wei.xiang@jcu.edu.au)

This work was supported in part by the National Science Foundation of China under Grant 61771106, in part by the National Key R&D Program of China under Grant 2018YFC0807101, and in part by the Science and Technology Department of Sichuan Province under Grant 2018GZ0092.

ABSTRACT Advanced wireless communications to support high vehicular speeds in the scenario of intelligent mobility have attracted considerable research attentions in both academia and industry. Multi-dimensional index modulation, which exploits transmission media resources for combining the concept of index modulation to achieve higher throughput with lower energy consumption, is regarded as a potential candidate for addressing the challenges in intelligent mobility communications. However, for the multi-dimensional index modulation system used in the mobile environment, the inter-carrier-interference (ICI) imposes a significant adverse impact on the system, especially in the context of multicarrier transmission. Therefore, by focusing on the two-dimensional index modulation system, the ICI impact on space-frequency index modulation is studied in this paper. Thanks to the grouping strategies and the Gaussian approximation to model the ICI, the approximate theoretical bounds for the error performance of the two dimensional systems are derived. Moreover, a novel robust space-frequency index modulation scheme is also developed. Finally, simulation results are presented to validate the system performances and the theoretical derivations.

INDEX TERMS Space-frequency index modulation, carrier frequency offset, inter-carrier interference.

I. INTRODUCTION

Future wireless communications are required to meet the needs of intelligent mobility, which requires high-volume and reliable data connections under high speed mobility. The Intelligent Mobility Communications means that the equipment in moving environment can sense the change of the state of the wireless channel and reconfigure the system to guarantee the quality of service via communicating. For example, as a high energy-efficient transportation option, smart rail provides a specific application scenario for 5G and beyond [1]–[3] , where wireless communications are expected to enable the wide-ranging data services, from operational services to in-flight-entertainment. However, high speed movement, up to 500 km/h for the high-speed train, in the application scenario with a high data throughput requirement makes the physical layer design an extreme challenge, as the 3GPP members have agreed to inherit the legacy of 4G and continue to utilize the orthogonal frequency-division multiplexing (OFDM) as the modulation scheme [4], [5], which is sensitive to the carrier frequency offset (CFO) [6]–[9]. The CFO incurred by high mobility may degrade the system performance significantly and the situation would be even worse if mmWave technology is deployed with carrier frequencies as high as 100 GHz [10]–[13]. How to address this challenge while utilizing existing wireless communication infrastructure is still an open issue.

Recently, muti-dimensional index modulation is emerging, which sheds some light on the challenging issue mentioned above [14]–[16]. Muti-dimensional index modulation provides an applicable scheme to embed the index modulation (IM) concept into the existing MIMO-OFDM system [17]. Therefore, future wireless communications can be realized by only updating the existing infrastructure instead of replacing it completely. Before investigating the ICI effects on multi-dimensional IM systems,

The associate editor coordinating the review of this manuscript and approving it for publication was Thomas Kuerner.

the evolution of the combination of IM and OFDM is briefly discussed.

The combination of the IM concept and OFDM technology can be traced back to the OFDM-IM system proposed in [18], which exploited the indices of the subcarriers in OFDM frames to convey additional information bits [19], [20]. As an extension of the OFDM-IM system, the generalized version of OFDM-IM was proposed in [21], where the interleaver was employed to improve the independence of subcarriers in OFDM-IM [22]. Moreover, the channel capacity of the OFDM-IM was investigated in [23], while the impact of the channel state information (CSI) uncertainty on OFDM-IM was analyzed in [24].

Following the OFDM-IM system, MIMO technology has been introduced to further improve the spectral efficiency leading to MIMO-OFDM-IM [25]. The results show that the MIMO-OFDM-IM system is able to improve the spectral efficiency compared to OFDM-IM systems and outperforms the conventional MIMO-OFDM system in terms of bit error rate (BER). However, the MIMO-OFDM-IM system has not fully exploited the index resource across the spatial and frequency domains, since it only uses the indices on the frequency domain to carry additional information bits and treats the transmit antenna independently when designing the transmit patterns.

To fully utilize the index resources over the spatial and frequency domains, some researchers have proposed to design the transmit patterns by jointly considering the indices in both the spatial and frequency domains. More specifically, in order to reduce the number of radio frequency (RF) links, the authors of [26] proposed the so-called generalized space-frequency index modulation (GSFIM), where antenna selection was applied before the joint space-frequency unit activation. Authors of [27] proposed two joint index modulation methods for the space-frequency domain, dubbed generalized joint space-frequency index modulation (G-JSFIM) and kronecker product-based joint space-frequency index modulation (KP-JSFIM), respectively. For G-JSFIM, IM is implemented directly in the space-frequency domain, while, for the KP-JSFIM system, the spatial and frequency indices are selected independently before a Kronecker product is used to determine the final active transmission units. The results showed that G-JSFIM can achieve better spectral efficiency (SE) than GSFIM, and KP-JSFIM outperforms MIMO-OFDM-IM in terms of the BER with reduced complexity. Furthermore, the IM concept implemented at the receiver side for MIMO-OFDM was studied in [28], where precoding technology was applied to use the indices at the receiver side to convey additional information bits. For higher dimension consideration, a more generalized IM approach to utilize space-time-frequency was proposed in [29].

However, considering the transmission environment of intelligent mobility communications, the aforementioned schemes may fail to combat the introduced ICI between the transmitter and receiver, which is a necessity for practical systems [30], [31]. In the application scenario with mobility, as OFDM systems are extremely sensitive to high CFO, the ICI induced by CFO will degrade the system performance significantly. In [32], index modulation is proposed for underwater communications with ICI and a novel CFO estimation scheme is proposed in [33]. An approximate union bound for the OFDM-IM with the ICI was derived in [34] by categorizing the ICI into two types, namely inter-subblock and intra-subblock ICIs and exploiting Gaussian approximation [35] to approximate inter-subblock ICI. Moreover, two spectral efficient index modulation schemes are proposed in [36] and in [37], sparse index modulation is proposed to relax the ICI effect. However, the current research only considered the influences on the SISO system and failed to appropriately address the ICI issue.

To our best knowledge, the impact of ICI on space-frequency IM systems has not been investigated in the literature to date. Therefore, we aim to make the following contributions in this paper. First of all, we propose a theoretical framework to quantify the influence of ICI introduced by CFO for space-frequency IM systems. Secondly, based on the analysis results, a novel index pattern generation scheme is proposed, which avoids activating the adjacent subcarriers in a group for each transmission, the theoretical and simulation results show that the proposed scheme can improve the error performance of the system under CFO effectively. Lastly, we give the simulation results to validate the theoretic analysis and the performance of the proposed scheme. The above-mentioned results have demonstrated and improved the effectiveness of the space-frequency IM system in the context of intelligent mobility communications.

The remainder of this paper is organized as follows. In Section II, the system model is presented. In Section III, the theoretical analysis for spatial-frequency IM under ICI is given and a novel transmit pattern design strategy is also proposed. Then, the simulation results are presented in Section IV. Finally, the conclusion is offered in Section V.

II. SYSTEM MODEL

Consider a system equipped with M transmit and N receive antennas. The transmit signals are generated as shown in Fig. 1 The OFDM frames are transmitted from each transmit antenna while the FFT size of the OFDM frames is L. Before applying the IM technique, each OFDM frame is partitioned into R groups. Therefore, there are $A = \frac{ML}{R}$ subcarriers in each group by jointly considering all the transmit antennas, and each transmit antenna contributes $B = \frac{L}{R}$ subcarriers to the joint spatial-frequency group. In each group, a subcarrier unit can be positioned by an index pair (b, m), where m is the index of the transmit antenna while b is the subcarrier index.

Assuming c bits are assigned to each group, the incoming bits are divided into two parts containing c_1 and c_2 bits, respectively, i.e., $c = c_1 + c_2$. The first c_1 bits are used to select a subcarrier activation pattern from the legitimate pattern set, i.e., $c_1 = C(A, K)$ where K is the number of active subcarriers in a group. The remaining c_2 bits are mapped to conventional amplitude phase modulation (APM)

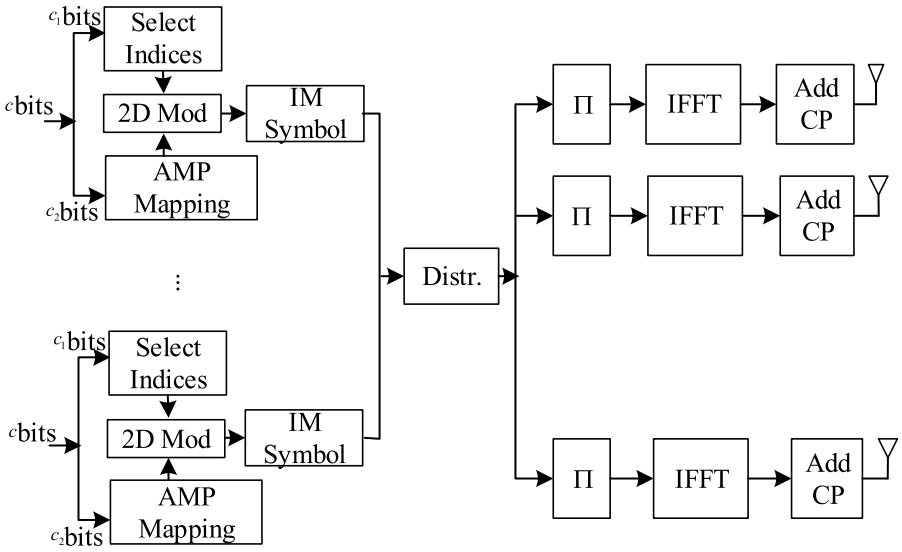

Fig. 1. The block diagram of the signal generation.

signals chosen from an $\mathcal{M}$-ary constellation. Without loss of generality, the transmit signal for the rth group $U_r \in \mathcal{C}^{B\times M}$ is chosen from the legitimate set ϕ with a cardinality of $|\phi| = 2^c$ and can be represented as

$$U_r = \sum_{k=1}^{K} s_{k,r}\, \Xi_{k,r} \tag{1}$$

where $s_{k,r}$ is the APM signal corresponding to the kth active unit in the rth group and $\Xi_{k,r} \in \{0, 1\}^{B\times M}$ is the indicator matrix with all 0s except for the element (b, m) corresponding to the kth active subcarrier set to 1.

Eq. (1) gives a general expression of the transmit signal in the joint space-frequency domain. Therefore, the SM-OFDM and MIMO-OFDM-IM systems can be regarded as two special cases which only use index resources in the spatial and frequency domains, respectively. For SM-OFDM, the transmit signal $u_r^s \in \mathcal{C}^{M\times 1}$ for the rth group can be given as

$$u_r^s = \sum_{k=1}^{K} s_{k,r}\xi_{k,r} \tag{2}$$

where the position of 1 in $\xi_{k,r} \in \{0, 1\}^{M\times 1}$ represents the location of the kth active transmit antenna in the spatial domain. Accordingly, the transmit signal $u_r^f \in \mathcal{C}^{B\times 1}$ for MIMO-OFDM-IM system can be given as

$$u_r^f = \sum_{k=1}^{K} s_{k,r}\xi_{k,r} \tag{3}$$

where the position of 1 in $\xi_{k,r} \in \{0, 1\}^{B\times 1}$ represents the location of the kth subcarrier in the frequency domain. Therefore, u_r^f can be viewed as the column of U_r, while $[u_r^s]^T$ can be viewed as the row component of U_r.

After modulation, R groups of transmit signals in frequency domain are concatenated to form $\tilde{U} = [U_1^T, U_2^T, \ldots, U_R^T]^T$ and distributed to M transmit antennas before passing through the normalized IFFT. After IFFT, a cyclic prefix (CP) is added. Furthermore, the interleaver Π_h could be used at the transmitter side to reap the diversity gain.

After the OFDM frames in the time domain are generated, the signals are sent over a frequency-selective Rayleigh fading MIMO channel. The channel has G_{ch} taps from the transmit antenna m to the receive antenna n in the time domain, whose elements are i.i.d Rayleigh random variables following the distribution $\mathcal{CN}(0, \frac{1}{G_{ch}})$. Then, the corresponding frequency domain fading from the transmit antenna m to the receive antenna n can be represented as

$$h_{nm} = [h_{1nm}, h_{2nm}, \cdots h_{Lnm}]^T, \tag{4}$$

where $h_{lnm} \in \mathbb{C}, l = 1, 2 \ldots L$ is the channel coefficient on subcarrier l. Since the FFT is linear, the channel fading coefficients in the frequency domain are still complex Gaussian random variables obeying $\mathcal{CN}(0, 1)$.

Let $\epsilon = \frac{f_d}{f_s}$ be the normalized CFO with doppler frequency f_d and subcarrier spacing f_s. Assuming the CFO on each receive antenna is identical and perfect channel state information and time synchronization are available at the receiver, the corresponding revived signals on the nth receive antenna in the frequency domain after removing the CP and deinterleaving is given by

$$\tilde{z}_n = \Theta \sum_{m=1}^{M} \mathrm{diag}(\tilde{h}_{nm})\tilde{U}_{:,m} + \tilde{w}_n^f \tag{5}$$

where

$$\Theta = \Pi_h \tilde{\Theta} \Pi_h^H \tag{6}$$

$$\tilde{\Theta} = FTF^H \tag{7}$$

are the ICI coefficients with and without interleaving, respectively. F is the normalized fast Fourier transform (FFT) matrix

$$F = \frac{1}{\sqrt{L}}[f_1, \ldots f_L] \tag{8}$$

and

$$f_i = [1, \exp(\frac{-j2\pi i}{L}) \ldots, \exp(\frac{-j2\pi i(L-1)}{L})]^T. \tag{9}$$

Π_h is the matrix corresponding to the employed interleaving and $\tilde{h}_{nm} = \Pi_h h_{nm}$ is the channel coefficient after deinterleaving. T is a diagonal matrix with the elements on its diagonal $T_{ii} = e^{\frac{j2\pi\epsilon(i-1)}{L}}$. $\tilde{U}_{:,m}$ is the mth column of $\tilde{U}$ and $\tilde{w}_n^f \in \mathcal{C}^{L\times 1}$ is the Gaussian noise in the frequency domain following the distribution $\mathcal{CN}(0, \delta_f^2)$. Moreover, as the normalized FFT is applied, the variances of noise in the time and frequency domains are identical.

III. PERFORMANCE ANALYSIS WITH ICI

In this section, the theoretical error performance for space-frequency IM with the CFO is derived and the transmitters with and without interleaving are both considered.

A. SFIM WITH INTERLEAVING

In this subsection, the theoretical error performance of space-frequency index modulation (SFIM) with interleavings is derived, where the CFO causes ICI. Based on the system model presented in Section II, the covariance matrix of the fading coefficients in the frequency domain between an arbitrary transmit-receive antenna pair $\{(n, m)|n = 1, 2 \ldots N, m = 1, 2, \ldots, M\}$ can be given as

$$J^{\Pi} = \mathrm{E}\{\tilde{h}_{nm}\tilde{h}_{nm}^H\} = \Pi_h F \tilde{I} F^H \Pi_h^H, \tag{10}$$

where

$$\tilde{I} = \begin{bmatrix} \frac{1}{G_{ch}} I_{G_{ch}} & 0_{G_{ch}\times(L-G_{ch})} \\ 0_{(L-G_{ch})\times G_{ch}} & 0_{(L-G_{ch})\times(L-G_{ch})} \end{bmatrix} \tag{11}$$

is the covariance matrix for the channel coefficients in the time domain.

Without loss of generality, in what follows, only the first group of the transmit SFIM signal is considered. Using the same strategy in [34], the ICI on the bth subcarrier of the first group on nth receive antenna can be categorized into two types, i.e., the intra-group ICI β_{bn}^1 and inter-group ICI β_{bn}^2. Moreover, the inter-group ICI can be approximated by a Gaussian random variable [35]. It is worth stressing that, the statistics we calculate in this paper are conditioned on the whole group channel fadings, i.e., $\{\tilde{h}_{1nm}, \tilde{h}_{2nm}, \ldots \tilde{h}_{Bnm}\}$ $n = 1, 2 \ldots N, m = 1, 2, \ldots, M\}$, which is different from [34]. Furthermore, different from [35], where only the SISO system with conventional digital modulation was considered, we investigate the SFIM system with MIMO channels and the concept of IM.

Denote by $d_{nm} = [\tilde{h}_{1nm}, \tilde{h}_{2nm}, \ldots \tilde{h}_{Bnm}]^T$ that channel coefficients corresponding to the subcarriers in the first group and $\bar{d}_{nm} = [\tilde{h}_{(B+1)nm}, \tilde{h}_{(B+2)nm}, \ldots \tilde{h}_{Lnm}]^T$ represent the remaining channel coefficients excluding the ones in the first group. Then, the joint covariance matrix can be partitioned as

$$J^{\Pi} = \begin{pmatrix} J_{dd}^{\Pi} & J_{d\bar{d}}^{\Pi} \\ J_{\bar{d}d}^{\Pi} & J_{\bar{d}\bar{d}}^{\Pi} \end{pmatrix}. \tag{12}$$

Under the assumption that the fadings on each transmit and receive antenna pair are independent and share the identical covariance, without ambiguity, the conditional expectation of the channel fading excluded from the first group can be given as

$$\mathrm{E}(\bar{d}_{nm}|d_{nm}) = J_{\bar{d}d}^{\Pi}(J_{dd}^{\Pi})^{-1} d_{nm}, \tag{13}$$

and the corresponding conditional variance can be represented as

$$\mathrm{Var}(\bar{d}_{nm}|d_{nm}) = \mathrm{Var}(\bar{d}|d) = J_{\bar{d}\bar{d}}^{\Pi} - J_{\bar{d}d}^{\Pi}(J_{dd}^{\Pi})^{-1}(J_{\bar{d}d}^{\Pi})^H. \tag{14}$$

The received signals for the first group $z_n \in \mathcal{C}^{B\times 1}$ on receive antenna n can be derived from (5) and reformulated as

$$z_n = \begin{bmatrix} \theta_{11}\sum_{m=1}^{M} \tilde{h}_{1nm}u_{1m} + \beta_{1n}^1 + \beta_{1n}^2 \\ \theta_{22}\sum_{m=1}^{M} \tilde{h}_{2nm}u_{2m} + \beta_{2n}^1 + \beta_{2n}^2 \\ \vdots \\ \theta_{BB}\sum_{m=1}^{M} \tilde{h}_{Bnm}u_{Bm} + \beta_{Bn}^1 + \beta_{Bn}^2 \end{bmatrix} + w_n^f, \tag{15}$$

where u_{bm} is the element of $\tilde{U}$. The intra-group ICI of subcarrier b on receive antenna n can be given as

$$\beta_{bn}^1 = \sum_{\substack{b'\in\Omega \\ b'\neq b}} \sum_{m=1}^{M} \theta_{bb'}\tilde{h}_{b'nm}u_{b'm}, \tag{16}$$

where $b \in \Omega = \{1, 2, \ldots, B\}$ and $\theta_{bb'}$ is the element in Θ corresponding to the ICI on subcarrier b from subcarrier b' after interleaving. The inter-group ICI on the bth subcarrier in the first group is written as

$$\beta_{bn}^2 = \sum_{b''\notin\Omega} \sum_{m=1}^{M} \theta_{bb''}\tilde{h}_{b''nm}u_{b''m}. \tag{17}$$

Let $\rho_b \in \mathcal{C}^{L\times 1}$ be the bth row of the ICI coefficient matrix Θ, which represents the ICI coefficients associated with the bth subcarrier. Using the same categorization strategy for channel fading, the ICI coefficients associated with the intra-group ICI to the bth subcarrier are given by

$$\rho_b = \{\theta_{bb'}|b, b' \in \Omega, b' \neq b\}, \tag{18}$$

while the corresponding coefficients of inter-group ICI for the bth subcarrier of the first group can be represented as $\bar{\rho}_b \in \mathcal{C}^{(L-B)\times 1}$ and $\bar{\rho}_b = \{\theta_{bb''}|b \in \Omega, b'' \notin \Omega\}$.

The pairwise error probability for the error event of the first group, where the detected signal is $\hat{U}$ when U is sent, is shown in (19) at the bottom of next page. $\hat{U}$ and U are the matrix representations for the transmit space-frequency

signals for the first group and $\hat{U}_{m,:} = \hat{u}_m$, $U_{m,:} = u_m$ $H = \{h_{nm}|n = 1, 2, \ldots N, m = 1, 2, \ldots, M\}$.

After Gaussian approximation, Eq. (19) reduces to

$$p(U \to \hat{U}|d) = P(2\mathcal{R}(v^H(\beta^2 + w^f)) > \|v\|^2 + 2\mathcal{R}(v^H\beta^1)) \quad (20)$$

where $d = [d_{11}^T, d_{12}^T, \ldots d_{NM}^T]^T$,$\beta^1 = [\beta_{11}^1, \beta_{21}^1, \ldots, \beta_{BN}^1]^T$ and $\beta^2 = [\beta_{11}^2, \beta_{21}^2, \ldots, \beta_{BN}^2]^T$ are the channel fading coefficients, intra-group and inter-group ICI associated with the first group for all receive antennas, respectively. The vector $v \in \mathcal{C}^{BN\times 1}$ can be given as

$$v = \begin{bmatrix} v_1^1 \\ \vdots \\ v_1^B \\ \vdots \\ v_N^1 \\ \\ v_N^B \end{bmatrix} = \begin{bmatrix} \sum_{m=1}^{M} \mathrm{diag}(d_{1m})(u_m - \hat{u}_m) \\ \vdots \\ \sum_{m=1}^{M} \mathrm{diag}(d_{Nm})(u_m - \hat{u}_m) \end{bmatrix}, \quad (21)$$

while the intra-group ICI vector β^1 can be written as

$$\beta^1 = \begin{bmatrix} \sum_{b'\in\Omega, b'\neq 1}^{M} \sum_{m=1}^{M} \theta_{1b'}\tilde{h}_{b'1m}u_{b'm} \\ \vdots \\ \sum_{b'\in\Omega, b'\neq B}^{M} \sum_{m=1}^{M} \theta_{Bb'}\tilde{h}_{b'1m}u_{b'm} \\ \vdots \\ \sum_{b'\in\Omega, b'\neq 1}^{M} \sum_{m=1}^{M} \theta_{1b'}\tilde{h}_{b'Nm}u_{b'm} \\ \vdots \\ \sum_{b'\in\Omega, b'\neq B}^{M} \sum_{m=1}^{M} \theta_{Bb'}\tilde{h}_{b'Nm}u_{b'm} \end{bmatrix}, \quad (22)$$

where $u_{b'm}$ are the signals contributing to the intra-group ICI.

Let $\bar{d}_{nm}|d_{mn} = d_{nm}^1 + d_{nm}^2$, where $d_{nm}^1 = \mathrm{E}(\bar{d}_{nm}|d_{nm})$ is associated with instantaneous channel coefficients d_{nm}, while $d_{nm}^2 = [d_{1nm}^2, d_{2nm}^2, \ldots, d_{(L-B)nm}^2]^T$ is unrelated to d_{nm} and $\mathrm{E}(|d_{inm}^2|^2) = (\mathrm{Var}(\bar{d}|d))_i$. Then, $x = \mathcal{R}(v^H\beta^2)$ can be represented as

$$x = \mathcal{R}(\sum_{n=1}^{N}\sum_{m=1}^{M}\sum_{b=1}^{B}\left(v_n^b\right)^H \bar{\rho}_b^T \mathrm{diag}(d_{nm}^1 + d_{nm}^2)\bar{u}_m), \quad (23)$$

where $\bar{u}_m$ is the OFDM signals sent from the transmit antenna m, excluding the subcarriers in the first group and v_n^b is the element in v, corresponding to the bth subcarrier in the first group for receive antenna n.

For BPSK, x and its variance can be obtained as (24) and (27) as shown at the bottom of the next page, respectively, where $(x)_i$ denotes the ith component of vector x and d_{inm}^1 , d_{inm}^2, $\bar{u}_{im}$ represent the ith element in d_{nm}^1, d_{nm}^1 and $\bar{u}_m$, respectively. Since the QPSK and other modulation schemes using both I and Q branches, x and its variance can be obtained in (28) and (29) as shown at the bottom of the next page, respectively.

Therefore, the conditional pairwise error probability in (19) can be represented as

$$p(U \to \hat{U}|d) = Q(\frac{\|v\|^2 + 2\mathcal{R}(v^H\beta^1)}{\sqrt{(\mathrm{Var}(x) + \|v\|^2\delta_f^2/2)}}) \quad (30)$$

where $d = \{d_{nm}|n = 1, 2\ldots, N, m = 1, 2, \ldots, M\}$ and $\mathrm{Var}(x)$ can be obtained via Eq. (27) or (29) according to the modulation style used. Then, the unconditional pairwise error probability can be simplified to

$$p(U \to \hat{U}) = \mathrm{E}(Q(\frac{\|v\|^2 + 2\mathcal{R}(v^H\beta^1)}{\sqrt{(\mathrm{Var}(x) + \|v\|^2\delta_f^2/2)}})). \quad (31)$$

Since (31) is very complex, the Monte Carlo method is utilized to attain results. Finally, the average error performance in terms of BER can be derived through the well-known Union Bound theory as

$$p_b = \frac{1}{c\,|\phi|}\sum_{U\in\phi}\sum_{\substack{\hat{U}\in\phi \\ \hat{U}\neq U}} p(U \to \hat{U})\mathrm{Ham}(U, \hat{U}), \quad (32)$$

where $\mathrm{Ham}(U, \hat{U})$ denotes the corresponding Hamming distance for the error event pair.

B. SFIM WITHOUT INTERLEAVING

In this section, the case without interleaving is considered. For this configuration, the covariance matrix for fading coefficients in the frequency domain is given as

$$J = E\{h_{nm}h_{nm}^H\} = FE\{q_{nm}q_{nm}^H\}F^H = F\tilde{I}F^H. \quad (33)$$

Focusing on the first group, as the subcarriers in the group are adjacent, the rank of the covariance matrix for the group is not full, i.e., $\mathrm{rank}(d_{nm}d_{nm}^H) < B$. Thanks to the high channel correlation in each group, the conditional expectation of the channel coefficients can be approximated as

$$\mathrm{E}(\bar{d}_{nm}|d_{nm}) \approx \mathrm{E}(\bar{d}_{nm}|d_{imn}) \quad (34)$$

where d_{imn} $i = \{1, 2, \ldots B\}$ represents the arbitrary subcarrier in the first group. Therefore, Eq. (34) can be rewritten as

$$\mathrm{E}(\bar{d}_{nm}|d_{imn}) = J_{d_{imn}d_{imn}}^{-1} J_{\bar{d}_{nm}|d_{imn}} d_{imn}. \quad (35)$$

$$p(U \to \hat{U}|H))) = P(\sum_{n=1}^{N}\left|z_n - \sum_{m=1}^{M}\mathrm{diag}(d_{nm})u_m\right|^2 > \sum_{n=1}^{N}\left|z_n - \sum_{m=1}^{M}\mathrm{diag}(d_{mn})\hat{u}_m\right|^2) \quad (19)$$

Furthermore, as the channel coefficient in the time domain obeys $\mathcal{CN}(0, \frac{1}{G})$, Eq. (35) can be further reduced to

$$\mathrm{E}(\bar{d}_{nm}|d_{imn}) = J_{\bar{d}_{nm}|d_{imn}} d_{imn}. \tag{36}$$

Accordingly, the variance of the conditional channel coefficients can be derived as

$$\begin{aligned} \mathrm{Var}(\bar{d}_{nm}|d_{nm}) &= \mathrm{Var}(\bar{d}_{nm}|d_{imn}) && (37)\\ &= J_{\bar{d}_{nm}\bar{d}_{nm}} - J_{\bar{d}_{nm}d_{imn}} J^{H}_{\bar{d}_{nm}d_{imn}}. && (38) \end{aligned}$$

By substituting $\mathrm{E}(\bar{d}_{nm}|d_{nm})$ and $\mathrm{Var}(\bar{d}_{nm}|d_{nm})$ in (24) and (29) with $\mathrm{E}(\bar{d}_{nm}|d_{imn})$ and $\mathrm{Var}(\bar{d}_{nm}|d_{imn})$ in (35) and (38), respectively, the theoretical error performance of the SFIM system without interleaving is attainable.

C. DEVELOPED ICI-ROBUST SFIM

After the derivation of the error performance of SFIM with ICI, it is evident that ICI is capable of degrading the system performance. Therefore, in this section, a novel strategy is developed to reduce ICI by exploiting the unique feature of IM. Since the nearest subcarrier contributes the most ICI, according to the results in (32), we propose to design the transmit index pattern by purposely avoiding the use of the subcarriers next to each other. That is, if the resource unit u_{bm} is activated, its nearest unit $u_{b'm'}$ must be kept silent, i.e.,

$$\begin{cases} u_{bm} = s_{bm} & u_{bm} \in \Lambda_i \\ u_{b'm'} = 0 & u_{b'm'} \in \Lambda_j,\ i \neq j \end{cases} \tag{39}$$

where $\{\Lambda_i\}$ is the set of groups of subcarriers in which $u_{bm} \in \Lambda_i$ while $u_{b'm'} \in \Lambda_j$ are not the adjacent subcarrier units when $i \neq j$.

For example, assuming the number of transmit antennas is $M = 2$ and the number of subcarriers contributed from each antenna to the group is $B = 4$, the legitimate space-frequency index patterns are depicted as Fig. 2, where the

$$x = \sum_{i=1}^{L-B}\sum_{m=1}^{M}\sum_{n=1}^{N}[\mathcal{R}((\sum_{b=1}^{B}\left(v_n^b\right)^H \bar{\rho}_b^T)_i)\mathcal{R}(d^1_{inm})) - \mathcal{I}((\sum_{b=1}^{B}\left(v_n^b\right)^H \bar{\rho}_b^T)_i)\mathcal{I}(d^1_{inm}) \tag{24}$$

$$+\mathcal{R}((\sum_{b=1}^{B}\left(v_n^b\right)^H \bar{\rho}_b^T)_i)\mathcal{R}(d^2_{inm}) - \mathcal{I}((\sum_{b=1}^{B}\left(v_n^b\right)^H \bar{\rho}_b^T)_i)\mathcal{I}(d^2_{inm})]\bar{u}_{im} \tag{25}$$

$$\mathrm{Var}(x) = \frac{K}{A}\sum_{i=1}^{L-B}\sum_{m=1}^{M}[(\sum_{n=1}^{N}\mathcal{R}[(\sum_{b=1}^{B}\left(v_n^b\right)^H \bar{\rho}_b^T)_i]\mathcal{R}(d^1_{inm}) - \mathcal{I}[(\sum_{b=1}^{B}\left(v_n^b\right)^H \bar{\rho}_b^T)_i]\mathcal{I}(d^1_{inm}))^2 \tag{26}$$

$$+\sum_{n=1}^{N}(\left(\mathcal{R}[(\left(v_n^b\right)^H \bar{\rho}_b^T)_i]\right)^2 \mathrm{E}(\left(\mathcal{R}(d^2_{inm})\right)^2) + \left(\mathcal{I}[(\left(v_n^b\right)^H \bar{\rho}_b^T)_i]\right)^2 \mathrm{E}(\left(\mathcal{I}(d^2_{inm})\right)^2)] \tag{27}$$

$$\begin{aligned} x = &\sum_{i=1}^{L-B}\sum_{m=1}^{M}\sum_{n=1}^{N}\mathcal{R}(\bar{u}_{im})[\mathcal{R}[(\sum_{b=1}^{B}\left(v_n^b\right)^H \bar{\rho}_b^T)_i]\mathcal{R}(d^1_{inm}) + \mathcal{R}[(\sum_{b=1}^{B}\left(v_n^b\right)^H \bar{\rho}_b^T)_i]\mathcal{R}(d^2_{inm})\\ &- \mathcal{I}[(\sum_{b=1}^{B}\left(v_n^b\right)^H \bar{\rho}_b^T)_i]\mathcal{I}(d^1_{inm}) - \mathcal{I}[(\sum_{b=1}^{B}\left(v_n^b\right)^H \bar{\rho}_b^T)_i]\mathcal{I}(d^2_{inm})]\\ &- \sum_{i=1}^{L-B}\sum_{m=1}^{M}\sum_{n=1}^{N}\mathcal{I}(\bar{u}_{im})[\mathcal{R}[(\sum_{b=1}^{B}\left(v_n^b\right)^H \bar{\rho}_b^T)_i]\mathcal{I}(d^1_{inm}) + \mathcal{R}[(\sum_{b=1}^{B}\left(v_n^b\right)^H \bar{\rho}_b^T)_i]\mathcal{I}(d^2_{inm})\\ &+\mathcal{I}[(\sum_{b=1}^{B}\left(v_n^b\right)^H \bar{\rho}_b^T)_i]\mathcal{R}(d^1_{inm}) + \mathcal{I}[(\sum_{b=1}^{B}\left(v_n^b\right)^H \bar{\rho}_b^T)_i]\mathcal{R}(d^2_{inm})] \end{aligned} \tag{28}$$

$$\begin{aligned} \mathrm{Var}(x) = &\frac{K}{2A}\sum_{i=1}^{L-B}\sum_{m=1}^{M}[(\sum_{n=1}^{N}(\mathcal{R}[(\sum_{b=1}^{B}\left(v_n^b\right)^H \bar{\rho}_b^T)_i]\mathcal{R}(d^1_{inm}) - \mathcal{I}[(\sum_{b=1}^{B}\left(v_n^b\right)^H \bar{\rho}_b^T)_i]\mathcal{I}(d^1_{inm})))^2\\ &+\sum_{n=1}^{N}((\mathcal{R}[(\sum_{b=1}^{B}\left(v_n^b\right)^H \bar{\rho}_b^T)_i])^2\mathrm{E}((\mathcal{R}(d^2_{inm}))^2) + (\mathcal{I}[(\sum_{b=1}^{B}\left(v_n^b\right)^H \bar{\rho}_b^T)_i])^2\mathrm{E}((\mathcal{I}(d^2_{inm})))^2)]\\ &+\frac{K}{2A}\sum_{i=1}^{L-B}\sum_{m=1}^{M}[(\sum_{n=1}^{N}(\mathcal{R}[(\sum_{b=1}^{B}\left(v_n^b\right)^H \bar{\rho}_b^T)_i]\mathcal{I}(d^1_{inm}) + \mathcal{I}[(\sum_{b=1}^{B}\left(v_n^b\right)^H \bar{\rho}_b^T)_i]\mathcal{R}(d^1_{inm})))^2\\ &+\sum_{n=1}^{N}(\mathcal{R}(\sum_{b=1}^{B}\left(v_n^b\right)^H \bar{\rho}_b^T)_i)^2\mathrm{E}((\mathcal{I}(d^2_{inm}))^2) + (\mathcal{I}[(\sum_{b=1}^{B}\left(v_n^b\right)^H \bar{\rho}_b^T)_i)^2\mathrm{E}((\mathcal{R}(d^2_{inm}))^2) \end{aligned} \tag{29}$$

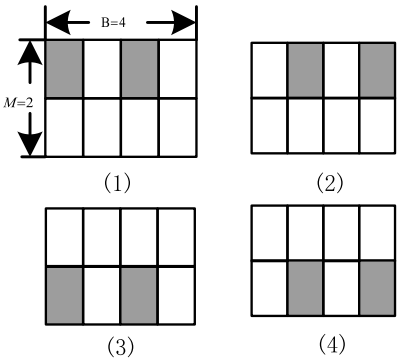

Fig. 2. Legitimate index patterns for ICI-robust SFIM.

TABLE 1. Mobility scenarios for different transmission configurations.

normalized CFO	velocity [km/h]
0.01	36
0.05	180
0.10	360
0.15	540
0.20	720

nearest subcarriers are not used simultaneously during a single transmission. More specifically, for the first legitimate index pattern, only the u_{11} and u_{31} units are activated. As can be seen from the simulation results shown in the next section, this low-cost index pattern design works effectively.

IV. SIMULATION

In this section, numerical simulations are carried out to validate the theoretical analysis. The system is configured as follows: $M = N = 2$, $L = 120$, $G_{ch} = G_{cp} = 8$, the error performances in terms of BER for the KP-JSFM system [27] are taken to validate the theoretic analysis. The systems with and without interleavers are both considered. Note that, although the simulations are carried out based on the KP-JSFM system, the analysis for the theoretic BER is applicable for all the other space-frequency index modulation schemes. Assuming carrier frequency $f = 4.5$ GHz and subcarrier spacing $f_s = 15$ kHz toward 5G systems, the velocities on intelligent mobility under different normalized CFO are presented in Table 1.

In Fig. 3, the theoretic and simulated BER results for KP-JSFIM with ICI and interleaving are exhibited. There are two subcarriers from each transmit antenna allocated to each group to achieve the spectral efficiency of 1.5 bits/s/Hz assuming BSPK is applied. It can be seen that ICI degrades KP-JSFIM performance significantly, since there is a 4dB loss in SNR at BER $= 10^{-3}$ when the normalized CFO $\epsilon = 0.15$. It is evident from the results that the derived theoretical bounds are tight for all ϵ values and mobility conditions.

In Fig. 4, the BER of KP-JSFIM with ICI and interleaves is depicted. QPSK is applied to achieve the spectral efficiency of 2 bits/s/Hz. As can be seen from the figure, the ICI influences the KP-JSFIM performance even more significantly.

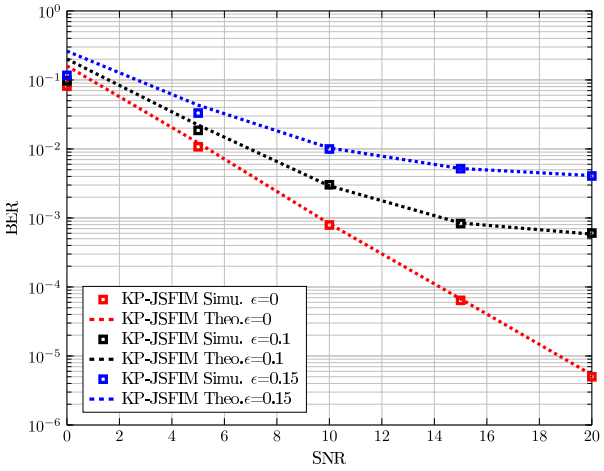

Fig. 3. BER of KP-JSFIM with ICI and interleaving, SE = 1.5 bits/s/Hz, BPSK.

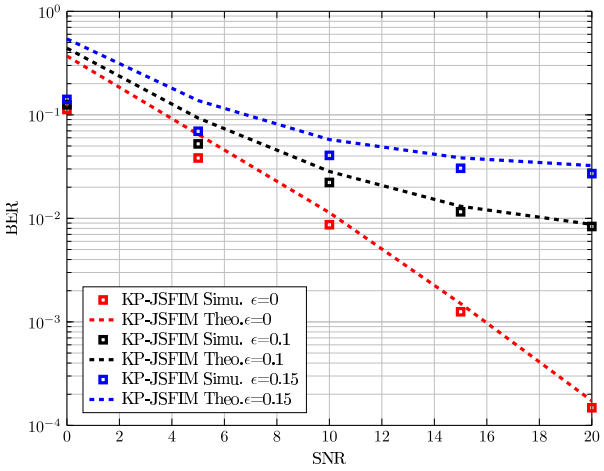

Fig. 4. BER of KP-JSFIM with ICI and interleavering, SE = 2 bits/s/Hz, QPSK.

There is approximately a 8dB loss in SNR at BER of 10^{-3} when the normalized CFO $\epsilon = 0.15$. This is due to the use of higher-order modulation schemes for KP-JSFIM, where ICI affects the detection of the APM signal severely. Again, the derived theoretic bounds are tight for various ϵ.

For space-frequency index modulation systems without the interleavers, the error performances of KP-JSFIM with ICI are given in Fig. 5 and 6 for spectral efficiencies 1.5 bits/s/Hz and 2 bits/s/Hz, respectively. More specifically, the theoretical and simulated BER results for KP-JSFIM with ICI and spectral efficiency of 1.5 bits/s/Hz are shown in Fig. 5. Compared with Fig. 3, it is evident that KP-JSFIM with interleaving outperforms its counterpart without interleaving. This is due to the fact that deploying the interleavers make the fading in each group more independent, which improve the index detection in the frequency domain. Although approximations are used in (34) and (35), the derived theoretical bounds are tight for all ϵ.

In Fig. 6, the theoretical and simulated BER results for KP-JSFIM with ICI and spectral efficiency of 2 bits/s/Hz are

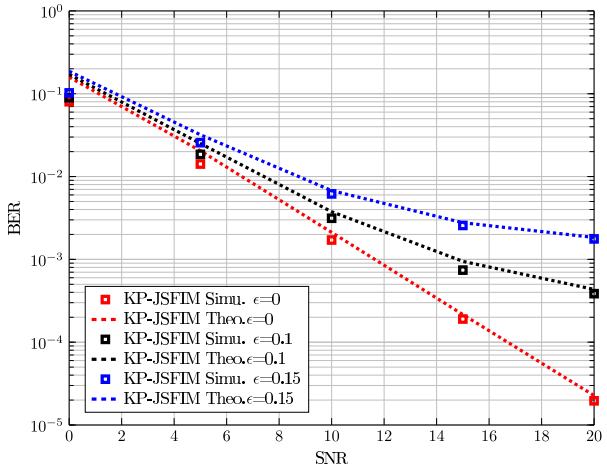

Fig. 5. BER of KP-JSFIM with ICI and without interleaving, SE = 1.5 bits/s/Hz, BPSK.

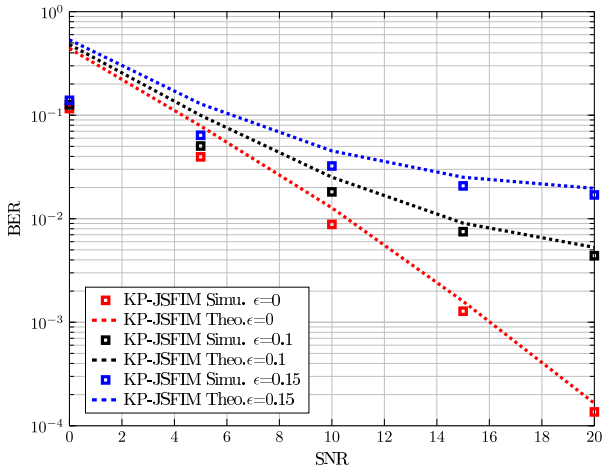

Fig. 6. BER of KP-JSFIM with ICI and without interleaving, SE = 2 bits/s/Hz, QPSK.

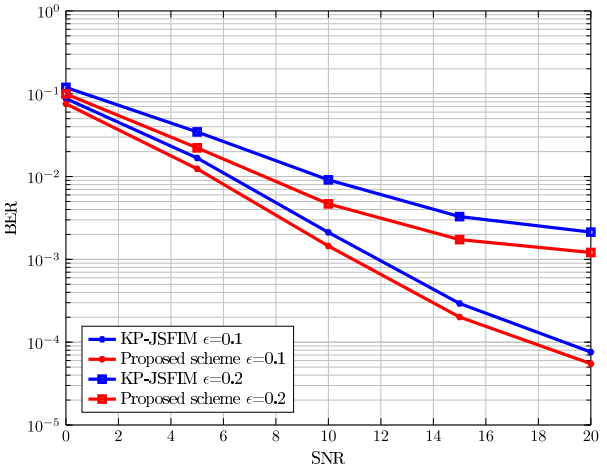

Fig. 7. BER comparison of the proposed scheme with KP-JSFIM B = 4.

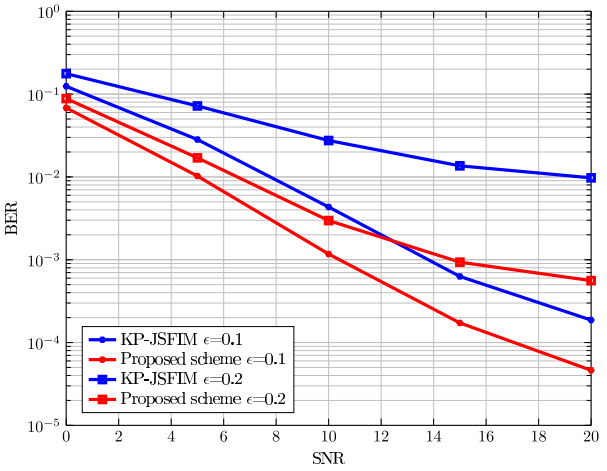

Fig. 8. BER comparison of the proposed scheme with KP-JSFIM, B = 6 .

shown. In accordance with the results shown in the previous figures, the derived theoretical bounds are very tight for all ϵ.

In Figs. 7 and 8, the proposed schemes are compared with KP-JSFIM with $B = 4$ and $B = 6$, respectively. In Fig. 7, four subcarriers from each transmit antenna are assigned to each group. It can be shown that the proposed schemes achieve approximate a SNR gain of 1dB at BER $= 10^{-3}$ with normalized $\epsilon = 0.1$, which is equivalent to the mobility speed up to 360 km/h when assuming the carrier frequency $f = 4.5$ GHz, $f_s = 15$ kHz. For $\epsilon = 0.2$, the proposed scheme reaps more than 2 dB SNR gain at BER $= 10^{-2}$. It is evident that, as the normalized CFO increases, the SNR gains attained by the proposed scheme increase as well. It shows that the proposed scheme can harvest more gains in the high mobility scenario, making it more suitable for high-mobility intelligent mobility communications.

In Fig. 8, the proposed schemes are compared to KP-JSFIM with $B = 6$. As can be observed from the figure, the proposed schemes improve the error performances under the influence of ICI significantly. More specifically, there is approximately an SNR gain of 5 dB at BER 10^{-3} for $\epsilon = 0.1$ i.e., 360 km/h and more than 8 dB gain for $\epsilon = 0.2$ at BER 10^{-2}. It can be seen that the proposed schemes have even better benefits with greater ICI, which shows its potential for intelligent communications.

V. CONCLUSION

In this paper, the impact of ICI on the space-frequency IM system has been studied. Although the combinatorial space is decreased, leading some minimal drop in terms of spectral efficiency, the proposed scheme enhances the transmit diversity of the system without increasing the number of transmit antennas. Therefore, it shows again that space-frequency index modulation is flexible to provide more design freedom to adapt to application scenarios.The theoretical error performance bounds were derived, considering its application in intelligent mobility communications with different system configurations. Based on the simulation results, the derived theoretical bounds were shown to be tight. Moreover, a novel ICI-robust index modulation scheme was proposed by exploring the unique feature of IM.We show that the developed

scheme is capable of improving the system error performance with the presence of ICI, for high-mobility intelligent communications. However, other factors, such as imperfect channel estimation and switching in high rate are still open issues and could be candidate topics in our future research work.

REFERENCES

[1] K. Guan, G. Li, T. Kurner, A. F. Molisch, B. Peng, R. He, B. Hui, J. Kim, and Z. Zhong, "On millimeter wave and THz mobile radio channel for smart rail mobility," *IEEE Trans. Veh. Technol.*, vol. 66, no. 7, pp. 5658–5674, Jul. 2017.
[2] K. Guan, B. Ai, B. Peng, D. He, X. Lin, L. Wang, Z. Zhong, and T. Kürner, "Scenario modules, ray-tracing simulations and analysis of millimetre wave and terahertz channels for smart rail mobility," *IET Microw., Antennas Propag.*, vol. 12, no. 4, pp. 501–508, Mar. 2018.
[3] P. Yang, Y. Xiao, M. Xiao, and S. Li, "6G wireless communications: Vision and potential techniques," *IEEE Netw.*, vol. 33, no. 4, pp. 70–75, Jul. 2019.
[4] A. Gupta and R. K. Jha, "A survey of 5G network: Architecture and emerging technologies," *IEEE Access*, vol. 3, pp. 1206–1232, 2015.
[5] M. Agiwal, A. Roy, and N. Saxena, "Next generation 5G wireless networks: A comprehensive survey," *IEEE Commun. Surveys Tuts.*, vol. 18, no. 3, pp. 1617–1655, Feb. 2016.
[6] T. Hwang, C. Yang, G. Wu, S. Li, and G. Ye Li, "OFDM and its wireless applications: A survey," *IEEE Trans. Veh. Technol.*, vol. 58, no. 4, pp. 1673–1694, May 2009.
[7] W.-S. Hou and B.-S. Chen, "ICI cancellation for OFDM communication systems in time-varying multipath fading channels," *IEEE Trans. Wireless Commun.*, vol. 4, no. 5, pp. 2100–2110, Sep. 2005.
[8] J. Lu, X. Chen, S. Liu, and P. Fan, "Location-aware ICI reduction in MIMO-OFDM downlinks for high-speed railway communication systems," *IEEE Trans. Veh. Technol.*, vol. 67, no. 4, pp. 2958–2972, Apr. 2018.
[9] J. Hao, J. Wang, and C. Pan, "Low complexity ICI mitigation for MIMO-OFDM in time-varying channels," *IEEE Trans. Broadcast.*, vol. 62, no. 3, pp. 727–735, Sep. 2016.
[10] Z. Xiao, P. Xia, and X.-G. Xia, "Codebook design for millimeter-wave channel estimation with hybrid precoding structure," *IEEE Trans. Wireless Commun.*, vol. 16, no. 1, pp. 141–153, Jan. 2017.
[11] P. Liu, M. Di Renzo, and A. Springer, "Line-of-sight spatial modulation for indoor mmWave communication at 60 GHz," *IEEE Trans. Wireless Commun.*, vol. 15, no. 11, pp. 7373–7389, Nov. 2016.
[12] X. Gao, L. Dai, S. Han, C.-L. I, and R. W. Heath, Jr., "Energy-efficient hybrid analog and digital precoding for MmWave MIMO systems with large antenna arrays," *IEEE J. Sel. Areas Commun.*, vol. 34, no. 4, pp. 998–1009, Apr. 2016.
[13] M. Kamel, W. Hamouda, and A. Youssef, "Ultra-dense networks: A survey," *IEEE Commun. Surveys Tuts.*, vol. 18, no. 4, pp. 2522–2545, May 2016.
[14] P. Yang, Y. Xiao, Y. L. Guan, M. Di Renzo, S. Li, and L. Hanzo, "Multidomain index modulation for vehicular and railway communications: A survey of novel techniques," *IEEE Veh. Technol. Mag.*, vol. 13, no. 3, pp. 124–134, Sep. 2018.
[15] E. Basar, "Index modulation techniques for 5G wireless networks," *IEEE Commun. Mag.*, vol. 54, no. 7, pp. 168–175, Jul. 2016.
[16] S. Sugiura, T. Ishihara, and M. Nakao, "State-of-the-art design of index modulation in the space, time, and frequency domains: Benefits and fundamental limitations," *IEEE Access*, vol. 5, pp. 21774–21790, 2017.
[17] E. Basar, "On multiple-input multiple-output OFDM with index modulation for next generation wireless networks," *IEEE Trans. Signal Process.*, vol. 64, no. 15, pp. 3868–3878, Aug. 2016.
[18] E. Basar, Ü. Aygölü, E. Panayirci, and H. V. Poor, "Orthogonal frequency division multiplexing with index modulation," *IEEE Trans. Signal Process.*, vol. 61, no. 22, pp. 5536–5549, Nov. 2013.
[19] E. Basar, M. Wen, R. Mesleh, M. Di Renzo, Y. Xiao, and H. Haas, "Index modulation techniques for next-generation wireless networks," *IEEE Access*, vol. 5, pp. 16693–16746, 2017.
[20] N. Ishikawa, S. Sugiura, and L. Hanzo, "Subcarrier-index modulation aided OFDM—Will it work?" *IEEE Access*, vol. 4, pp. 2580–2593, 2016.
[21] R. Fan, Y. J. Yu, and Y. L. Guan, "Generalization of orthogonal frequency division multiplexing with index modulation," *IEEE Trans. Wireless Commun.*, vol. 14, no. 10, pp. 5350–5359, Oct. 2015.
[22] Y. Xiao, S. Wang, L. Dan, X. Lei, P. Yang, and W. Xiang, "OFDM with interleaved subcarrier-index modulation," *IEEE Commun. Lett.*, vol. 18, no. 8, pp. 1447–1450, Aug. 2014.
[23] M. Wen, X. Cheng, M. Ma, B. Jiao, and H. V. Poor, "On the achievable rate of OFDM with index modulation," *IEEE Trans. Signal Process.*, vol. 64, no. 8, pp. 1919–1932, Apr. 2016.
[24] T. Van Luong and Y. Ko, "Impact of CSI uncertainty on MCIK-OFDM: Tight closed-form symbol error probability analysis," *IEEE Trans. Veh. Technol.*, vol. 67, no. 2, pp. 1272–1279, Feb. 2018.
[25] E. Basar, "Multiple-input multiple-output OFDM with index modulation," *IEEE Signal Process. Lett.*, vol. 22, no. 12, pp. 2259–2263, Dec. 2015.
[26] T. Datta, H. S. Eshwaraiah, and A. Chockalingam, "Generalized space-and-frequency index modulation," *IEEE Trans. Veh. Technol.*, vol. 65, no. 7, pp. 4911–4924, Jul. 2016.
[27] R. Chen and J. Zheng, "Index-modulated MIMO-OFDM: Joint space-frequency signal design and linear precoding in rapidly time-varying channels," *IEEE Trans. Wireless Commun.*, vol. 17, no. 10, pp. 7067–7079, Oct. 2018.
[28] S. Gao, M. Zhang, and X. Cheng, "Precoded index modulation for multi-input multi-output OFDM," *IEEE Trans. Wireless Commun.*, vol. 17, no. 1, pp. 17–28, Jan. 2018.
[29] M. I. Kadir, "Generalized space-time-frequency index modulation," *IEEE Commun. Lett.*, vol. 23, no. 2, pp. 250–253, Feb. 2019.
[30] B. Ai, X. Cheng, T. Kürner, Z.-D. Zhong, K. Guan, R.-S. He, L. Xiong, D. W. Matolak, D. G. Michelson, and C. Briso-Rodriguez, "Challenges toward wireless communications for high-speed railway," *IEEE Trans. Intell. Transp. Syst.*, vol. 15, no. 5, pp. 2143–2158, Oct. 2014.
[31] J. Moreno, J. M. Riera, L. D. Haro, and C. Rodriguez, "A survey on future railway radio communications services: Challenges and opportunities," *IEEE Commun. Mag.*, vol. 53, no. 10, pp. 62–68, Oct. 2015.
[32] M. Wen, X. Cheng, L. Yang, Y. Li, X. Cheng, and F. Ji, "Index modulated OFDM for underwater acoustic communications," *IEEE Commun. Mag.*, vol. 54, no. 5, pp. 132–137, May 2016.
[33] Z. Yang, F. Chen, B. Zheng, M. Wen, and W. Yu, "Carrier frequency offset estimation for OFDM with generalized index modulation systems using inactive data tones," *IEEE Commun. Lett.*, vol. 22, no. 11, pp. 2302–2305, Nov. 2018.
[34] Q. Ma, P. Yang, Y. Xiao, H. Bai, and S. Li, "Error probability analysis of OFDM-IM with carrier frequency offset," *IEEE Commun. Lett.*, vol. 20, no. 12, pp. 2434–2437, Dec. 2016.
[35] L. Rugini and P. Banelli, "BER of OFDM systems impaired by carrier frequency offset in multipath fading channels," *IEEE Trans. Wireless Commun.*, vol. 4, no. 5, pp. 2279–2288, Sep. 2005.
[36] H. S. Hussein, M. Elsayed, U. S. Mohamed, H. Esmaiel, and E. M. Mohamed, "Spectral efficient spatial modulation techniques," *IEEE Access*, vol. 7, pp. 1454–1469, 2019.
[37] M. Salah, O. A. Omer, and U. S. Mohammed, "Spectral efficiency enhancement based on sparsely indexed modulation for green radio communication," *IEEE Access*, vol. 7, pp. 31913–31925, 2019.

RUI CAO received the B.S. and M.S. degrees from the University of Electronic Science and Technology of China (UESTC), in 2005 and 2008, respectively. He is currently pursuing the Ph.D. degree with the National Key Laboratory of Science and Technology on Communications. His main research interests include index modulation systems, precoding, and performance analysis of wireless communications.

XIA LEI received the Ph.D. degree in communication and information systems from the University of Electronic Science and Technology of China, Chengdu, China, in 2005. She is currently a Professor and the Supervisor of Ph.D. students with University of Electronic Science and Technology of China. She has published more than 60 international journals. Her major research interests are mobile communication, multicarrier techniques, and cooperative wireless communications.

YUE XIAO received the Ph.D. degree in communication and information systems from the University of Electronic Science and Technology of China (UESTC), in 2007. He is currently a Professor with the National Key Laboratory of Science and Technology on Communications, UESTC. He has published more than 100 international journals. He has been in charge of more than 20 projects in the area of Chinese 3G/4G/5G wireless communication systems. He is also an inventor of more than 50 Chinese and PCT patents on wireless systems. His research interests are in system design and signal processing toward future wireless communication systems. He also serves as an Associate Editor of the IEEE COMMUNICATIONS LETTERS.

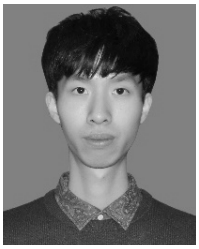

YOU LI received the B.S. degree in communication and information systems from the University of Electronic Science and Technology of China (UESTC), in 2013, where he is currently pursuing the Ph.D. degree with the National Key Laboratory of Science and Technology on Communications. His research interest includes spatial modulation toward future wireless communication systems.

WEI XIANG received the B.Eng. and M.Eng. degrees in electronic engineering from the University of Electronic Science and Technology of China, Chengdu, China, in 1997 and 2000, respectively, and the Ph.D. degree in telecommunications engineering from the University of South Australia, Adelaide, SA, Australia, in 2004. From 2004 to 2015, he was with the School of Mechanical and Electrical Engineering, University of Southern Queensland, Toowoomba, QLD, Australia. From August 2012 and March 2013, he was an Endeavour Visiting Associate Professor with the University of Hong Kong. He is currently a Foundation Professor and the Head of electronic systems and the Internet of Things engineering with the College of Science and Engineering, James Cook University, Cairns, QLD, Australia. He has published more than 160 articles in peer-reviewed journal articles and conference papers. His research interests are in the broad area of communications and information theory, particularly coding, and signal processing for multimedia communications systems. He is an IET Fellow and a Fellow of Engineers Australia. He has been awarded several prestigious fellowship titles. He was named a Queensland International Fellow by the Queensland Government of Australia, from 2010 to 2011, an Endeavour Research Fellow by the Commonwealth Government of Australia, from 2012 to 2013, a Smart Futures Fellow by the Queensland Government of Australia, from 2012 to 2015, and a JSPS Invitational Fellow jointly by the Australian Academy of Science and Japanese Society for Promotion of Science, from 2014 to 2015. He was a co-recipient of three best paper awards at the 2015 WCSP, the 2011 IEEE WCNC, and the 2009 ICWMC. In 2008, he was a Visiting Scholar with Nanyang Technological University, Singapore. From October 2010 and March 2011, he was a Visiting Scholar with the University of Mississippi, Oxford, MS, USA. He is also an Editor of the IEEE COMMUNICATIONS LETTERS.